

Jammed disks of two sizes and weights in a channel: alternating sequences

Dan Liu¹ and Gerhard Müller²

¹ *Department of Physics, University of Hartford, West Hartford, CT 06117, USA*

² *Department of Physics, University of Rhode Island, Kingston RI 02881, USA*

Disks of two sizes and weights in alternating sequence are confined to a long and narrow channel. The axis of the channel is horizontal and its plane vertical. The channel is closed off by pistons that freeze jammed microstates out of loose disk configurations subject to moderate pressure, gravity, and random agitations. Disk sizes and channel width are such that under jamming no disk remains loose and all disks touch one wall. We present exact results for the characterization of jammed macrostates including volume and entropy. The rigorous analysis divides the disk sequences of jammed microstates into overlapping tiles out of which we construct a small number of species of statistically interacting particles. Jammed macrostates depend on dimensionless control parameters inferred from ratios between measures of expansion work against the pistons, gravitational potential energy, and intensity of random agitations. These control parameters enter the configurational statistics via the activation energies prior to jamming of the particles. The range of disk weights naturally divides into regimes where qualitatively different features come into play. We sketch a path toward generalizations that include random sequences under a modified jamming protocol.

I. INTRODUCTION

The physics of jammed granular matter is dominated by experimental studies [1–13] and computational studies [14–37] more than is the cases in many other areas of condensed matter physics. The advanced computational power now available for simulations of granular matter subject to diverse protocols of athermal agitations and jamming has efficiently aided the interpretation of existing measurements and has inspired alternative experimental probes. The wealth of phenomena, too rich in scope to be listed here, has been reviewed from a range of perspectives [38–45].

Theoretical approaches operating under the umbrella of *configurational statistics* [46–53] have carved out comparably small corners in this wide field of research which permit an exact analysis or systematic approximations of some scenarios by specifically designed methodologies [54–62]. One such corner involves jammed matter in narrow channels [63–71], where the diversity of jammed configurations is limited by *caging effects* [37]. Nevertheless, the constrained quarters of granular matter in narrow channels leave ample room for complex phenomena and promising routes for the further development of methods of exact analysis.

The research reported in this work builds on two previous studies [70, 71], in which jammed granular matter in a narrow channel is represented by configurations of statistically interacting particles and amenable to exact analysis by methods of statistical mechanics developed in different contexts [72–80] and adapted to configurational statistics. Their focus was on the ordering tendencies of jammed disks of one size and weight, confined to a narrow channel and subject to combinations of gravity, friction, and centrifugation.

Here we consider configurations of jammed disks with two different sizes and two different weights, which adds diversity to the observed phenomena. More importantly, this generalization is a way station toward the investi-

gation of random configurations of disks with different sizes and weights. Exact results for a random sequence of jammed disks with two sizes and weights thus move well within reach in the wake of this study.

The key step that makes this progress possible is a twofold shift in the entities subjected to configurational statistics, (i) from disks to tiles and (ii) from tiles to statistically interacting particles. Step (i) was already taken in Refs. [65–67]. Step (ii) was developed in Refs. [70, 71] for disks of one size and is here generalized to situations involving disks of two sizes. The analysis is laid out in a way that facilitates further generalizations to random sequences of such disks.

The methodology presented here for jammed granular matter is far from common and it is not yet clear where it will reach its limitations. It will remain promising for as long as it produces new exact results of interest. Interestingly, the same methodology also yields new exact results in applications to quantum gases [81], to quantum spin chains embedded in solids [82], and to biological matter including polypeptides [83] and DNA [84].

The configurational statistics of disks with two different sizes and/or weights jammed in a channel includes ingredients related to geometry (Sec. II), energetics (Sec. III), combinatorics (Sec. IV), and statistical mechanics (Sec. V) to be worked out up front and then assembled. We discuss each ingredient in the context of the simplest application, where the weights of small and large disks are in balance (Sec. VI), and then use them again for applications, where size and weight produce more complex patterns (Secs. VII and VIII).

In the absence of gravitational effects, the statistical mechanics can be carried out with just two species of particles instead of five (Sec. IX). We conclude by pointing the way toward a generalization of this work which includes jammed macrostates of random sequences of disks with two sizes and weights. The modified jamming protocol permits disks to move past each other in a widened channel during random agitations (Sec. X).

II. GEOMETRY

Disks of two sizes with diameters $\sigma_L \geq \sigma_S$ in alternating sequence are being jammed in a channel of width H . Every jammed disk has three points of contact, either with an adjacent disk or with a wall. The constraints,

$$\frac{1}{4} < \frac{\sigma_S}{\sigma_L} \leq 1, \quad (1a)$$

$$1 < \frac{H}{\sigma_L} < \frac{1}{2} \left[1 + \frac{\sigma_S}{\sigma_L} + \sqrt{\left(1 + \frac{\sigma_S}{\sigma_L}\right)^2 - 1} \right], \quad (1b)$$

guarantee that the disk sequence remains invariant before jamming at constant H , that all jammed disks have wall contact, and that no loose disks exist under jamming. In the one-size limit $\sigma_S/\sigma_L \rightarrow 1$, condition (1b) reduces to the condition, $1 < H/\sigma < 1 + \sqrt{3}/4$, familiar from Ref. [70].

All jammed microstates can be assembled from 8 tiles composed of two adjacent disks similar to domino pieces (Table I), with a one-disk overlap. Adding a tile to an already existing string must satisfy two successor rules: The tile added must (i) match the pattern regarding size and position of the overlapping disk and (ii) maintain mechanical stability under jamming forces. Each tile has one of two distinct volumes (Table II).

TABLE I: Distinct tiles that constitute jammed microstates of alternating disk sequences subject to the constraints (1). Mechanical stability rule: v must be followed by w or 2 etc. Motifs pertain to $\sigma_L = 2$, $\sigma_S = 1.4$, $H = 2.5$.

motif	ID	rule	vol.	motif	ID	rule	vol.
	v	w, 2	V_c		3	v	V_f
	w	v, 1	V_c		4	5, 6	V_c
	1	3, 4	V_f		5	3, 4	V_c
	2	5	V_f		6	w, 2	V_f

TABLE II: Volume of tiles (with unit cross section). The numerical values are for $\sigma_L = 2$, $\sigma_S = 1.4$, $H = 2.5$.

	vol.	num.
V_c	$\frac{1}{2}(\sigma_L + \sigma_S) + \sqrt{H(\sigma_L + \sigma_S - H)}$	3.2
V_f	$\frac{1}{2}(\sigma_L + \sigma_S) + \sqrt{\sigma_L \sigma_S}$	3.373

Next we choose a convenient jammed reference state and generate other jammed microstates via the activation of quasiparticles which modify the reference state.

III. ENERGETICS

With no loss of generality regarding macrostates, we assume to have N (large/small) pairs of disks in the channel with the first (large) disk and the last (small) disk fixed in the (vertical) positions of tile v . Under these assumptions the microstate of minimum volume is unique. It is composed of an alternating sequence of just two tiles:

$$pv = vwwv \cdots v. \quad (2)$$

We declare it to be the pseudo-vacuum for statistically interacting particles in this application. All other (jammed) microstates can be generated by the activation of quasi-particles from this reference state. We have identified $M = 5$ species of particles that serve this purpose (Table III). Adopting the taxonomy of [78] we distinguish between the categories of hosts and tags.

TABLE III: Five species of quasi-particles. The hosts $m = 1, \dots, 4$ modify the pseudo-vacuum (2) whereas the tag $m = 5$ modifies any one of the hosts. The motifs shown are for $\sigma_L = 2$, $\sigma_S = 1.4$, $H = 2.5$. The ID lists the sequence of tiles that make the particle. The excess volume is ΔV_m and the activation energy ϵ_m .

motif	ID	m	cat.	ΔV_m	ϵ_m
	13	1	host	$2V_t$	$2pV_t - \gamma_S$
	146	2	host	$2V_t$	$2pV_t - \gamma_S + \gamma_L$
	253	3	host	$2V_t$	$2pV_t - \gamma_S + \gamma_L$
	2546	4	host	$2V_t$	$2pV_t - \gamma_S + 2\gamma_L$
	45	5	tag	0	$\gamma_L - \gamma_S$

Each particle consists of overlapping tiles. Particles from species $m = 1, \dots, 4$ can be placed directly into the pseudo-vacuum, meaning that it is possible to add a tile v or w to the left or to the right as follows:

$$w13v, \quad w146w, \quad v253v, \quad v2546w. \quad (3)$$

Particles from species $m = 5$ are parasitic in the sense that they can only be placed inside a particle from species $m = 1, \dots, 4$, at exactly one position and with one disk overlapping:

$$1|45|3, \quad 1|45|46, \quad 25|45|3, \quad 25|45|46. \quad (4)$$

The number of tag particles that can be added (at the same position in the same host) is only limited by the size of the system. For example, two tags inside the first host reads $1|4545|3$. The minimum number of tiles v or w between two hosts can be two as in $13vw146$, one as in $13v13$, or zero as in 146253 .

The activation of every host particle extends the volume between the piston by the amount $\Delta V = 2V_t$, where

$$V_t \doteq V_f - V_c = \sqrt{\sigma_L \sigma_S} - \sqrt{H(\sigma_L + \sigma_S - H)}. \quad (5)$$

Placing a tag, by contrast, does not change the volume.

The activation energy ϵ_m assigned to a particle from species m pertains to the state of random agitation before jamming. It consists of work against the ambient pressure exerted by the pistons and gravitational potential energy, all relative to the pseudo-vacuum. We are free to choose the mass density of small and large disks. Therefore, the gravitational potential energies γ_L and γ_S are independent parameters as is the expansion work $2pV_t$.

A fourth parameter is the intensity of random agitations, denoted T_k in analogy to the intensity $k_B T$ of thermal fluctuations. All results coming out of configurational statistics will only depend on the following three (dimensionless) ratios of these four energetic parameters:

$$\beta \doteq \frac{2pV_t}{T_k}, \quad \Gamma_L \doteq \frac{\gamma_L}{2pV_t}, \quad \Gamma_S \doteq \frac{\gamma_S}{2pV_t}. \quad (6)$$

The particle composition of a macrostate thus depends on the energetics prior to jamming. The multiplicity of microstates that characterize a macrostate of given particle composition is the solution of a combinatorial problem.

IV. COMBINATORICS

The quasi-particles identified in Table III are statistically interacting in the sense that activating one particle affects the number d_m of remaining slots for the activation of further particles from each species. This effect can be accounted for by a generalized Pauli principle [72] in the form [70, 78],

$$d_m = A_m - \sum_{m'=1}^M g_{mm'} (N_{m'} - \delta_{mm'}), \quad (7)$$

with capacity constants A_m and statistical interaction coefficients $g_{mm'}$ as listed in Table IV, and where N_m is the number of activated particles from species m .

The initial capacity for hosts grows linearly with the number of disks in the channel. It is zero for tags, which can only be activated inside hosts. Activating a host ($m' = 1, \dots, 4$) removes one or two slots for activating a further host ($m = 1, \dots, 4$) but adds one slot for activating a tag ($m = 5$). Activating a tag ($m' = 5$) removes one slot for activating hosts ($m = 1, \dots, 4$) but leaves the number of slots for activating a further tag ($m = 5$) invariant.

The multiplicity of jammed microstates with particle content $\{N_m\}$ is a product of binomials:

$$W(\{N_m\}) = \prod_{m=1}^M \binom{d_m + N_m - 1}{N_m}. \quad (8)$$

We now have all the ingredients for the statistical mechanical analysis as was developed previously [70, 73, 74].

TABLE IV: Capacity constants A_m and statistical interaction coefficients $g_{mm'}$ for the particles from Table III.

m	A_m	$g_{mm'}$	1	2	3	4	5
1	$N - 2$	1	2	2	1	2	1
2	$N - 3$	2	1	2	1	1	1
3	$N - 2$	3	2	2	2	2	1
4	$N - 3$	4	1	2	1	2	1
5	0	5	-1	-1	-1	-1	0

V. STATISTICAL MECHANICS

We can express both the excess volume and the entropy as functions of the average particle content $\{\langle N_m \rangle\}$ of a jammed macrostate as follows [74]:

$$V - V_{pv} = \sum_{m=1}^M \langle N_m \rangle \Delta V_m, \quad (9)$$

$$S = k_B \sum_{m=1}^M \left[(\langle N_m \rangle + Y_m) \ln (\langle N_m \rangle + Y_m) - \langle N_m \rangle \ln \langle N_m \rangle - Y_m \ln Y_m \right], \quad (10a)$$

$$Y_m \doteq A_m - \sum_{m'=1}^M g_{mm'} \langle N_{m'} \rangle. \quad (10b)$$

The average particle numbers are the solutions of the linear equations [73, 74],

$$w_m \langle N_m \rangle + \sum_{m'=1}^M g_{mm'} \langle N_{m'} \rangle = A_m. \quad (11)$$

The auxiliary quantities w_m are the non-negative set of solutions of the algebraic equations [73, 74],

$$e^{\epsilon_m/T_k} = (1 + w_m) \prod_{m'=1}^M (1 + w_{m'}^{-1})^{-g_{m'm}}. \quad (12)$$

The only parts that depend on the jamming protocol, i.e. on the three dimensionless parameters (6) are the exponents on the left. The analytic solution of Eqs. (12) is, in general, too unwieldy for display. Its availability gives us explicit expressions for the scaled excess volume, the scaled entropy, and the particle densities,

$$\bar{V} \doteq \frac{V - V_{pv}}{2NV_t}, \quad \bar{S} \doteq \frac{S}{Nk_B}, \quad \bar{N}_m \doteq \frac{\langle N_m \rangle}{N}, \quad (13)$$

as functions of $\beta, \Gamma_L, \Gamma_S$, representing, as noted in the context of (6), the (inverse) intensity of random agitations and the gravitational potential energies of large and small disks, all in units of expansion work against the pistons before jamming.

VI. WEIGHTS IN BALANCE

We begin our presentation of results at the border between the two regimes of heavy and light large disks (briefly reported in Ref. [85]). When we declare

$$\Gamma_L = \Gamma_S \doteq \Gamma \quad (14)$$

to hold, it means that the gravitational potential energies of large and small disks are equal when they touch the same wall. This equality removes the effect of gravity from the activation energies of the particles from species $m = 2, 3, 5$. On either side of this border, gravity favors qualitatively different jamming patterns as we shall see. Neither matches the pattern right on the border.

In Fig. 1 we show the population densities \bar{N}_m plotted versus β for all five species of particles at different values of Γ . Recall that increasing β means reducing the intensity of random agitations before jamming and increasing Γ means increasing the effects of gravity (by reducing the ambient pressure before jamming [86]).

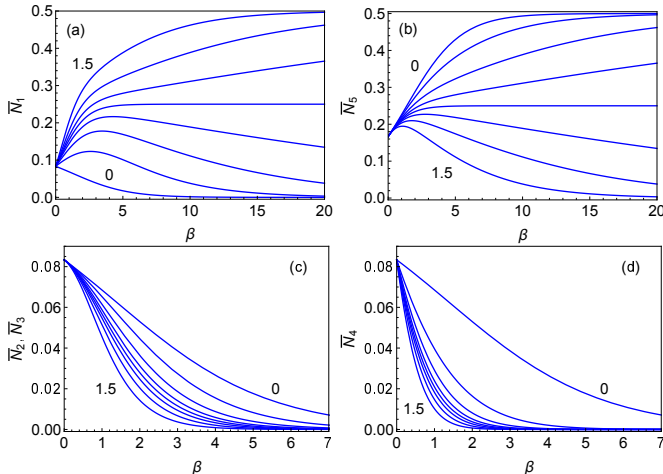


FIG. 1: Population densities (a) \bar{N}_1 , (b) \bar{N}_5 , (c) $\bar{N}_2 = \bar{N}_3$, (d) \bar{N}_4 versus parameter β for fixed parameter values $\Gamma = 0, 0.5, 0.75, 0.9, 1.0, 1.1, 1.25, 1.5$.

In the high-intensity limit, we have

$$\bar{N}_1 = \dots = \bar{N}_4 = \frac{1}{12}, \quad \bar{N}_5 = \frac{1}{6} \quad : \quad \beta = 0. \quad (15)$$

The contributions of species $m = 2, 3, 4$ quickly fade away as β increases from zero. That trend is aided by gravity. The two dominant species, $m = 1, 5$, are a host/tag pair with tags 5 existing inside hosts 1 in arbitrary numbers and with only hosts contributing to excess volume.

For weak gravity, $\Gamma < 1$, the host population, \bar{N}_1 , initially increases and then approaches zero as β increases. For strong gravity, $\Gamma > 1$, it increases monotonically toward the asymptotic value, $\bar{N}_1 = \frac{1}{2}$. The trends are roughly opposite for the tag population density, \bar{N}_5 . At

the border between these two regimes, $\Gamma = 1$, both population densities level off at $\bar{N}_1 = \bar{N}_5 = \frac{1}{4}$ in the low-intensity limit $\beta \rightarrow \infty$.

The effects of particle population densities on the excess volume and entropy of jammed macrostates are governed by Eqs. (9) and (10), respectively, and shown in Fig. 2 (for fewer values of Γ). In the high-intensity limit, we thus infer from (15) the values,

$$\bar{V} = \frac{2}{3}, \quad \bar{S} = \ln 3 \quad : \quad \beta = 0, \quad (16)$$

for excess volume and entropy of the most disordered macrostate.

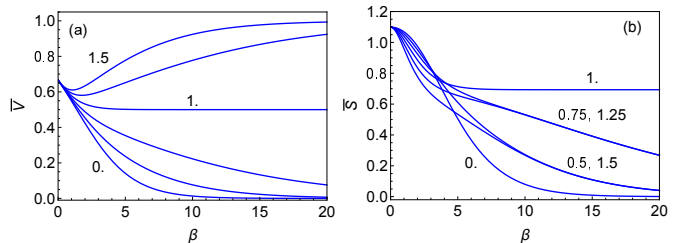


FIG. 2: (a) Excess volume \bar{V} and (b) entropy \bar{S} versus parameter β for fixed values $\Gamma = 0, 0.5, 0.75, 1.0, 1.25, 1.5$.

As β increases, the excess volume initially goes down no matter whether gravity is weak or strong [panel (a)]. If gravity is weak it continues to do go down and vanishes asymptotically for $\beta \rightarrow \infty$. For strong gravity, on the other hand, the downward trend is quickly reversed into an upward trend toward the asymptotic value $\bar{V} = 1$.

Irrespective of whether the intensity reduction of random agitations before jamming leads to larger or smaller volume, it always leads to lower entropy [panel (b)]. The entropy approaches zero at rates which vary a great deal with Γ . The ordered state being approached for $\Gamma < 1$ is different from the one approached for $\Gamma > 1$. The quickest approach by far to the ordered jammed state pertains to the zero-gravity case.

The borderline case, $\Gamma = 1$, is exceptional. The intensity reduction does not lead to an ordered jammed state. The excess volume settles at an intermediate value and the entropy at a nonzero value:

$$\lim_{\beta \rightarrow \infty} \bar{V} = \frac{1}{2}, \quad \lim_{\beta \rightarrow \infty} \bar{S} = \ln 2 \quad : \quad \Gamma = 1. \quad (17)$$

In order to better understand the roles of the different particle species, we plot the population densities versus volume [Fig. 3]. In these parametric plots, the high-intensity limit $\beta = 0$ is realized at point *A* for hosts and point *B* for tags. Increasing β toward infinity means moving along any path toward one or the other of two corners in each panel, depending on whether $\Gamma \gtrless 1$. In the exceptional case $\Gamma = 1$, all paths stop at $\bar{V} = \frac{1}{2}$.

An important fact about the case (14) of balanced gravity is that the overall population density of particles

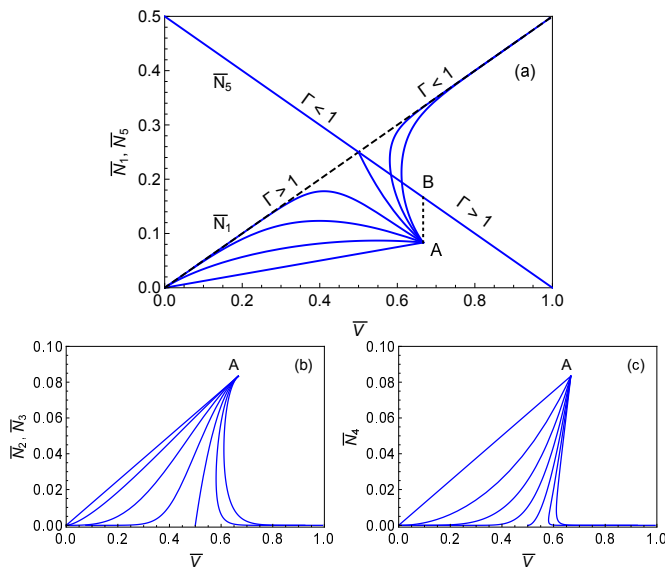


FIG. 3: Population densities \bar{N}_m , $m = 1, \dots, 5$ versus excess volume \bar{V} for fixed values $\Gamma = 0, 0.25, 0.5, 0.75, 1.0, 1.25, 1.5$ from bottom up in panel (a) and from left to right in panels (b) and (c). The dotted line connects the points pertaining to $\beta = 0$ for hosts and tags. The dashed diagonal represents the sum $\bar{N}_1 + \bar{N}_2 + \bar{N}_3 + \bar{N}_4$.

is an invariant:

$$\bar{N}_{\text{tot}} \doteq \sum_{m=1}^5 \bar{N}_m = \frac{1}{2} = \text{const.} \quad (18)$$

This is illustrated by the two diagonal lines in Fig. 3(a), where the dashed line represents the population density of all hosts combined. Recall that the tags $m = 5$ do not contribute to excess volume. Their numbers are determined, nevertheless, by the excess volume via the conservation law. Any increase in volume caused by the activation of one or the other host necessarily crowds out one tag. The curves in Fig. 3 again highlight the observation made earlier that hosts $m = 2, 3, 4$ only contribute significantly at high intensity.

It is instructive to take a closer look at the three distinct macrostates associated with $\beta = \infty$. All have $\bar{N}_2 = \bar{N}_3 = \bar{N}_4 = 0$.

(i) $\Gamma < 1$: The state with $\bar{N}_1 = 0$ and $\bar{N}_5 = \frac{1}{2}$ is realized and has $\bar{V} = 0$, $\bar{S} = 0$. It is a doublet consisting of the reference state (2) and the state 14545...4546. The former is free of particles. The latter contains one host 2 with a saturated number of tags 5 inside.

(ii) $\Gamma > 1$: The state with $\bar{N}_1 = \frac{1}{2}$ and $\bar{N}_5 = 0$ is realized and has $\bar{V} = 1$, $\bar{S} = 0$. It is a singlet packed with hosts 1: 13vw13vw...13v. Hosts 1 proliferate because they have negative activation energies.

(iii) $\Gamma = 1$: The state with $\bar{N}_1 = \bar{N}_5 = \frac{1}{4}$ is realized and has $\bar{V} = \frac{1}{2}$, $\bar{S} = \ln 2$. It is highly degenerate. The hosts 1 are randomly distributed between vacuum tiles with a random number of tags inside. Hosts 1 and tags

5 have zero activation energies, whereas the hosts, 2, 3, 4 have positive activation energies.

With this information we are ready to interpret a graphical representation of entropy versus excess energy [Fig. 4]. The parameter β runs from zero to infinity along each path from the top down. All paths start at coordinates (16). Paths for $\Gamma < 1$ end at $\bar{V} = 0$, $\bar{S} = 0$, and paths for $\Gamma > 1$ at $\bar{V} = 1$, $\bar{S} = 0$. At critical gravity, $\Gamma = 1$, both volume, the path ends at coordinates (17).

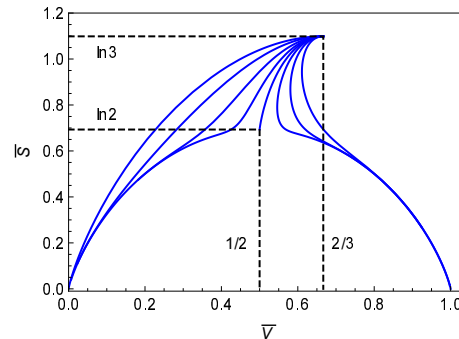


FIG. 4: Entropy \bar{S} versus excess volume \bar{V} for fixed values $\Gamma = 0, 0.5, 0.75, 0.9, 1.0, 1.1, 1.25, 1.5$ (from left to right).

Compact analytic expressions for the curves in Figs. 3 and 4 are available for the cases of zero and critical gravity. In the case $\Gamma = 0$ we have

$$\bar{N}_1 = \dots = \bar{N}_4 = \frac{1}{8}\bar{V}, \quad \bar{N}_5 = \frac{1}{2}(1 - \bar{V}), \quad (19a)$$

$$\bar{S} = (\bar{V} - 1) \ln \left(\frac{2}{\bar{V}} - 2 \right) + \ln \left(\frac{2}{\bar{V}} \right), \quad (19b)$$

where the range of volume is $0 \leq \bar{V} \leq \frac{2}{3}$. In the case $\Gamma = 1$ we have

$$\bar{N}_1 = \frac{(\bar{V} - 1)^2}{2\bar{V}}, \quad \bar{N}_2 = \bar{N}_3 = \frac{3}{2} - \bar{V} - \frac{1}{2\bar{V}}, \quad (20a)$$

$$\bar{N}_4 = 2\bar{V} + \frac{1}{2\bar{V}} - 2, \quad \bar{N}_5 = \frac{1}{2}(1 - \bar{V}), \quad (20b)$$

$$\bar{S} = 2(\bar{V} - 1) \ln \left(\frac{1 - \bar{V}}{2\bar{V} - 1} \right) - \ln(2\bar{V} - 1), \quad (20c)$$

across the more restricted range $\frac{1}{2} \leq \bar{V} \leq \frac{2}{3}$ of volume.

VII. HEAVY LARGE DISKS

Next we discuss the case where the large disks are heavier than the small disks in the sense that

$$\Gamma_L > \Gamma_S \quad (21)$$

All graphs for this case use $\Gamma_L = 2\Gamma_S$. In the following, we merely point out the main differences from the weights-in-balance case.

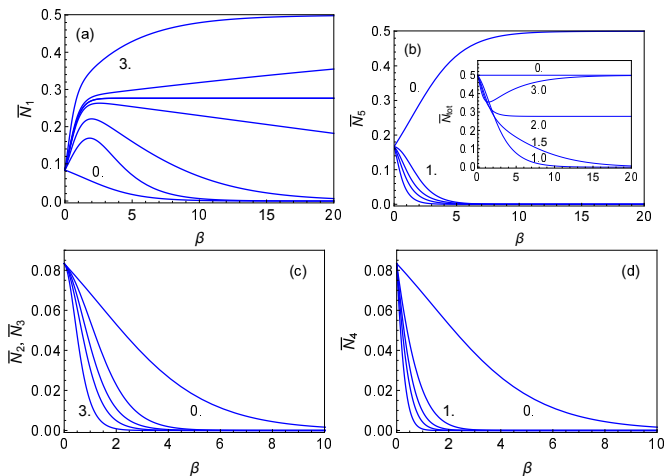


FIG. 5: Population densities (a) \bar{N}_1 , (b) \bar{N}_5 , (c) $\bar{N}_2 = \bar{N}_3$, (d) \bar{N}_4 versus parameter β for fixed values $\Gamma_L = 0, 1.0, 1.5, [1.9], 2.0, [2.1], 3.0$. The inset shows \bar{N}_{tot} versus β .

The particle population densities \bar{N}_m plotted versus β [Fig. 5] look similar with one notable exception. The role of tags is greatly diminished for any $\Gamma_L > 0$. This has the consequence that jamming with reduced intensity of random agitations produces macrostates dominated by hosts 1 alone. There are again regimes of strong and weak gravity with criticality now at $\Gamma_L = 2$. We find

$$\lim_{\beta \rightarrow \infty} \bar{N}_1 = \begin{cases} 0 & : \Gamma_L < 2, \\ \frac{1}{10}(5 - \sqrt{5}) & : \Gamma_L = 2, \\ \frac{1}{2} & : \Gamma_L > 2, \end{cases} \quad (22)$$

The overall particle content was the invariant (18) for weights in balance. This quantity now varies with β as shown in the inset to Fig. 5(b). Only for $\Gamma_L = 0$ is it still an invariant. Turning on gravity precipitates significant changes.

For weak gravity, $0 < \Gamma_L < 2$, reducing the intensity of random agitations has the consequence of depleting the system of particles gradually and completely. Asymptotically for $\beta \rightarrow \infty$, the jammed macrostate becomes the pseudo-vacuum. At strong gravity, $\Gamma_L > 2$, the particle content also begins to go down but then turns around and returns to the initial value asymptotically for $\beta \rightarrow \infty$. Initially, all particles are present in the proportions (15), finally it's all hosts 1. For the case $\Gamma_L = 2$, the particle content goes down as well, but levels off as stated in (22), again representing hosts 1 alone.

The dependence on β of volume and entropy remain qualitatively the same [Fig. 6] as before, but with different asymptotics at the border $\Gamma_L = 2$ between the two regimes:

$$\lim_{\beta \rightarrow \infty} \bar{V} = 1 - \frac{1}{\sqrt{5}} \simeq 0.553 \quad : \Gamma_L = 2, \quad (23a)$$

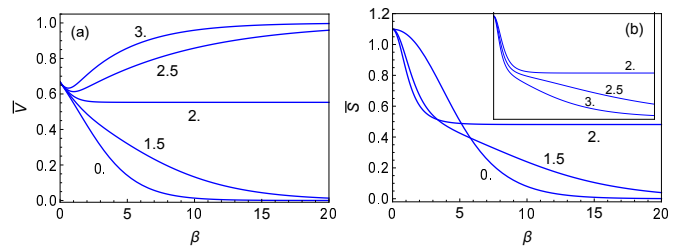


FIG. 6: (a) Excess volume \bar{V} and (b) entropy \bar{S} versus parameter β for fixed values $\Gamma_L = 0, 1.0, 1.5, 2.0, 2.5, 3.0$.

$$\lim_{\beta \rightarrow \infty} \bar{S} = \frac{1}{2} \ln \left(\frac{1}{2} (3 + \sqrt{5}) \right) \simeq 0.481. \quad (23b)$$

The diminished role of tags 5 is again highlighted in Fig. 7, where the population densities are plotted versus excess volume \bar{V} . Panel (a) also shows the overall particle content. Along two of the curves there are short segments along which the system loses particles while the volume of the jammed state increases. Changes occur also in two of the macrostates associated with $\beta = \infty$ (all with $\bar{N}_2 = \bar{N}_3 = \bar{N}_4 = \bar{N}_5 = 0$).

(i) $0 < \Gamma_L < 2$: The state realized is the reference state, which (by construction) contains no particles and has $\bar{V} = 0$ and $\bar{S} = 0$.

(ii) $\Gamma_L > 2$: The state realized is a close-packed array of hosts, implying $\bar{N}_1 = \frac{1}{2}$, $\bar{V} = 1$, and $\bar{S} = 0$ as we have encountered in the strong-gravity regime (Sec. VI).

(iii) $\Gamma_L = 2$: The state realized is again highly degenerate and thus carries entropy but unlike in Sec. VI it contains only hosts. Their average density is higher, $\bar{N}_1 \simeq 0.276$, but they are shorter for lack of tags.

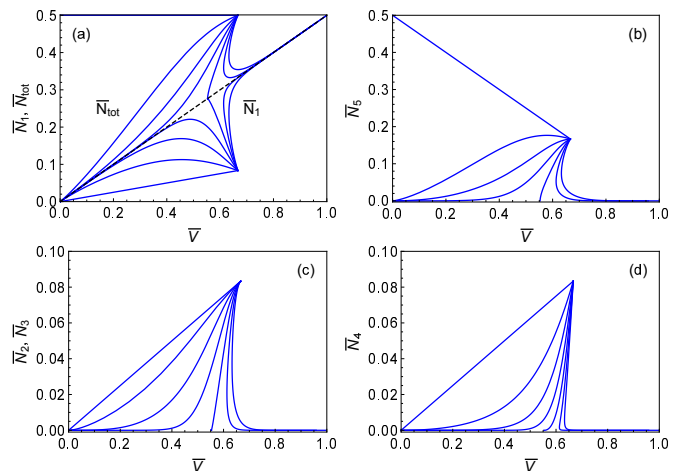


FIG. 7: Population densities \bar{N}_m , $m = 1, \dots, 5$ and \bar{N}_{tot} versus excess volume \bar{V} for fixed values $\Gamma_L = 0, 0.5, 1.0, 1.5, 2.0, 2.5, 3.0$ [\bar{N}_1 from bottom up, $\bar{N}_{\text{tot}}, \bar{N}_5$ from top down, $\bar{N}_2, \bar{N}_3, \bar{N}_4$ from left to right.] The dashed diagonal represents the sum $\bar{N}_1 + \bar{N}_2 + \bar{N}_3 + \bar{N}_4$.

It is perhaps surprising that all the changes we have noted between this case of heavy large disks and the previous case of weights in balance produce a mere distortion when we plot entropy versus volume [Fig. 8]. One of the landmarks in the plot has the same coordinates (16), the other is somewhat shifted from (17) to (23).

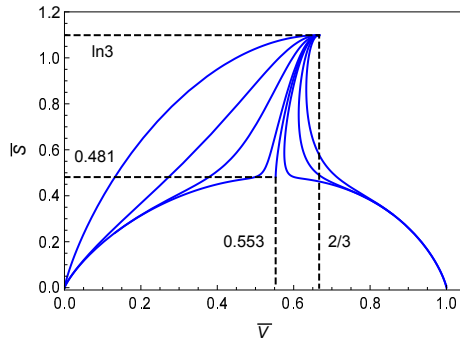


FIG. 8: Entropy \bar{S} versus excess volume \bar{V} for fixed values $\Gamma_L = 0, 1.0, 1.5, 1.8, 2.0, 2.2, 2.5, 3.0$ (from left to right).

VIII. LIGHT LARGE DISKS

If the weights of large and small disks are oppositely unbalanced, in the sense that

$$\Gamma_L < \Gamma_S, \quad (24)$$

then jamming produces yet different results. There are two regimes with different ordering patterns. We first discuss the borderline case, which involves subtle limits, and then one case on either side of the border.

A. $\Gamma_L = \frac{1}{2}\Gamma_S$.

The hallmark of this case is the presence of distinct weak-gravity and strong-gravity jamming patterns with a crossover between them upon variation of the intensity of random agitations before jamming. The clearest evidence is seen in plots of \bar{V} and \bar{S} versus β [Fig. 9].

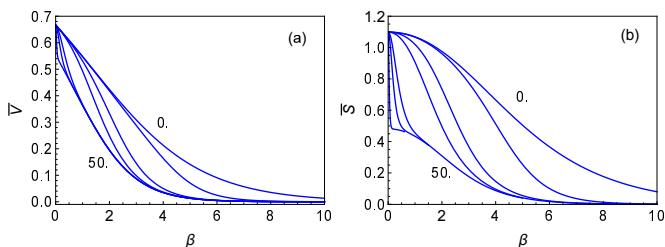


FIG. 9: (a) Excess volume \bar{V} and (b) entropy \bar{S} versus β for fixed values $\Gamma_L = 0, 0.1, 0.5, 1, 5, 10, 50$.

In both panels the top curve represents zero gravity and the bottom curve very strong gravity. For intermediate strengths of gravity, the curves initially follow the zero-gravity behavior and then, with increasing β , cross over to the strong gravity behavior. For large values of Γ_L , the crossover turns into a transition that destabilizes the zero-gravity behavior for all $\beta > 0$. A discontinuity emerges in the combined but non-interchangeable limits $\Gamma_L \rightarrow \infty, \beta \rightarrow 0$ between the most disordered macrostate with values (16),

$$\lim_{\Gamma_L \rightarrow \infty} \lim_{\beta \rightarrow 0} \bar{V} = \frac{2}{3} \simeq 0.667, \quad (25a)$$

$$\lim_{\Gamma_L \rightarrow \infty} \lim_{\beta \rightarrow 0} \bar{S} = \ln 3 \simeq 1.099, \quad (25b)$$

and the partially ordered macrostate with values,

$$\lim_{\beta \rightarrow 0} \lim_{\Gamma_L \rightarrow \infty} \bar{V} = 1 - \frac{1}{\sqrt{5}} \simeq 0.553, \quad (26a)$$

$$\lim_{\beta \rightarrow 0} \lim_{\Gamma_L \rightarrow \infty} \bar{S} = \frac{1}{2} \ln \left(\frac{1}{2} (3 + \sqrt{5}) \right) \simeq 0.481. \quad (26b)$$

This two-stage process of ordering in the jammed macrostate produced by random agitations of diminishing intensity has its characteristic signatures in the particle population densities [Fig. 10]. During the first stage, the populations of hosts 1 and tags 5 are enhanced whereas hosts 2,3,4 become extinct. During the second stage, hosts 1 disappear gradually whereas the population of tags 5 gradually increases toward its maximum value. The particle population overall, \bar{N}_{tot} , increases monotonically with increasing β [inset]. With increasing Γ_L , the first stage becomes more and more abrupt, whereas the second stage remains gradual.

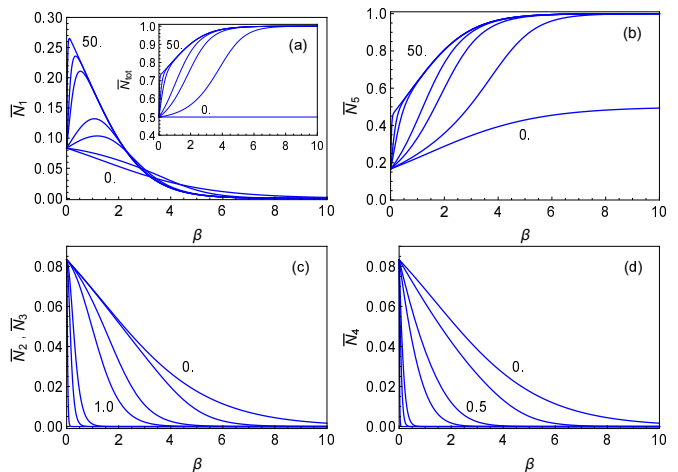


FIG. 10: Population densities (a) \bar{N}_1 , (b) \bar{N}_5 , (c) $\bar{N}_2 = \bar{N}_3$, (d) \bar{N}_4 versus β for fixed values $\Gamma_L = 0, 0.1, 0.5, 1, 5, 10, 50$.

The signature plot, \bar{S} versus \bar{V} , for this case is shown in Fig. 11. The dashed lines from Fig. 8, remain relevant. Weak gravity initially has roughly the same effect in the two cases represented by Figs. 8 and 11. For light large disks and infinitely strong gravity, $\Gamma_L \rightarrow \infty$, the path of macrostates during the first stage quickly transitions from coordinates (25) to (26). The latter are identical to coordinates (23) in Fig. 8, where they specify a macrostate in the limit $\beta \rightarrow \infty$.

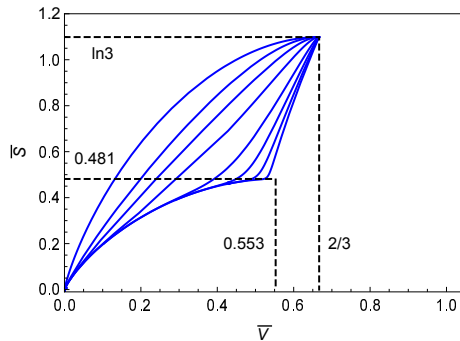


FIG. 11: Entropy \bar{S} versus excess volume \bar{V} for fixed values $\Gamma_L = 0, 0.5, 1, 2, 5, 10, 20, 50$ (from left to right).

The macrostate with $\bar{V} = 0$ and $\bar{S} = 0$ arrived at in the limit $\beta \rightarrow \infty$ is a singlet made of one host 2 packed with tags 5: 14545...4546. The macrostate (26) contains hosts 1 with $\bar{N}_1 \simeq 0.276$ randomly distributed between vacuum tiles, and tags 5 with $\bar{N}_5 \simeq 0.447$ randomly distributed among the hosts.

The two macrostates with the same coordinates, (23) in Fig. 8 and (26) in Fig. 11, are very different in particle composition. The former only contain hosts 1, whereas the latter contains hosts 1 and tags 5. The former (latter) is realized for very weak (strong) random agitations before jamming.

How do we explain that these two macrostates with different particle composition have the same excess volume and the same entropy? Only hosts carry excess volume. Both macrostates contain the same number of hosts, hence produce the same \bar{V} . Hosts alone are smaller in size and the size is unique. Hosts with tags are larger in size but the sizes are many. Hosts with tags have fewer options for placement between them, which subtracts entropy, but they produce distinguishable permutations, which adds entropy. This is no explanation, but an argument in support of plausibility.

B. $\Gamma_L = \frac{1}{3}\Gamma_S$.

This case of very light large disks exhibits the least complex behavior. It resembles the borderline case in some aspects and differs in others. For $\Gamma_L > 0$, all host populations are suppressed eventually as $\beta \rightarrow \infty$ and the tag population grows to its maximum value [Fig. 12].

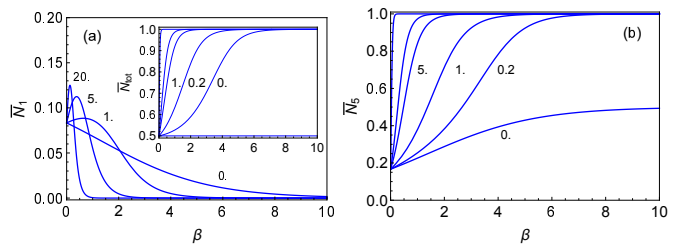


FIG. 12: Population densities versus β (a) \bar{N}_1 for $\Gamma_S = 0, 1, 5, 20$, (b) \bar{N}_5 for $\Gamma_S = 0, 0.2, 1, 5, 10, 100$. The inset shows \bar{N}_{tot} for $\Gamma_S = 0, 0.2, 1, 5, 10, 100$.

Only hosts 1 show hints of a two stage process emerging as Γ_L becomes large: a quick initial rise followed by an equally fast drop. Compared to the case of Sec. VIII A, the second stage is now much faster in the event of strong gravity. The variation of excess volume and entropy with β (not shown) is equally fast and all downward.

The plot of \bar{S} versus \bar{V} [Fig. 13] shows no complexity but is informative nevertheless. We observe that the relation between excess volume and entropy becomes increasingly linear as gravity becomes stronger. The only way to interpret this is that in the limit $\Gamma_L \rightarrow \infty$ both quantities collapse discontinuously to zero as β becomes nonzero. The initial macrostate has maximum disorder. The final state is the same singlet as identified in Sec. VIII A.

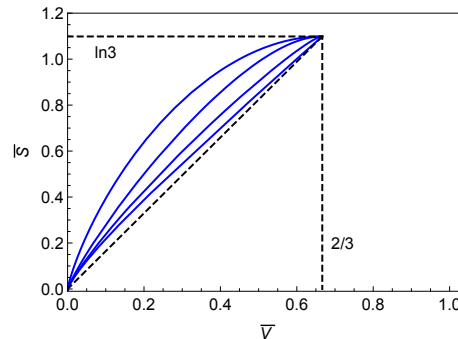


FIG. 13: Entropy \bar{S} versus excess volume \bar{V} for $\Gamma_S = 0, 1, 5, 100$ (from left to right).

C. $\Gamma_L = \frac{2}{3}\Gamma_S$.

On the other side of the borderline case, where the large disks are not much lighter than the small disks, the jamming patterns are more varied. We can state (without showing evidence) that all particle population densities vary less precipitously with β than in the preceding two cases. However, turning on gravity produces an abrupt change in the (average) particle composition of the jammed macrostate. Further abrupt changes occur when gravity crosses criticality at $\Gamma_L = 2$.

These changes are best illustrated in plots of particle population densities versus excess volume [Fig. 14] We have noted before (Sec. VI) that the jammed macrostate at zero gravity is a doublet in the limit $\beta \rightarrow \infty$. Increasing Γ_L from zero removes that degeneracy, which has the effect that the (average) tag population density doubles. For $\Gamma_L < 2$ the effect of increasing β is that the population of hosts 1 first increases and then decreases toward zero [panel (a)]. The populations of the other three hosts decrease from the start at $\beta = 0$ [panels (c) and (d)] such that the excess volume is a monotonically decreasing function. The overall population density of particles is, on the other hand is monotonically increasing [panel (e)] on account of the population increase of tags 5 [panel (b)].

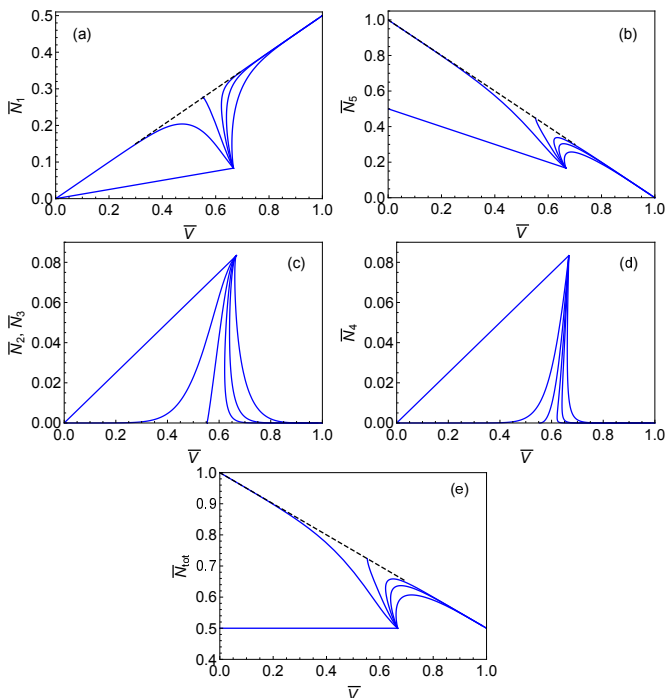


FIG. 14: Population densities \bar{N}_m , $m = 1, \dots, 5$ and \bar{N}_{tot} versus excess volume \bar{V} for fixed values $\Gamma_S = 0, 2, 3, 4, 5, 10$ (from left to right).

For critical gravity, $\Gamma_L = 2$, the effect of increasing β is that the population densities of hosts 1 and tags 5 both increase whereas those of the remaining hosts vanish gradually as in all cases. The macrostate in the limit $\beta \rightarrow \infty$ is a familiar one, encountered before in the case of heavy large disks, namely the disordered state with the values (23) for excess volume and entropy.

For stronger gravity, $\Gamma_L > 2$, the particle composition of the jammed macrostate approaches an ordered state again in the limit $\beta \rightarrow \infty$. This state is packed with hosts 1 and has the maximum excess volume as also seen in the case of heavy large disks. Note that as β increases, the population of hosts 2,3,4 initially depletes more rapidly than the population of hosts 1 increases, which has the

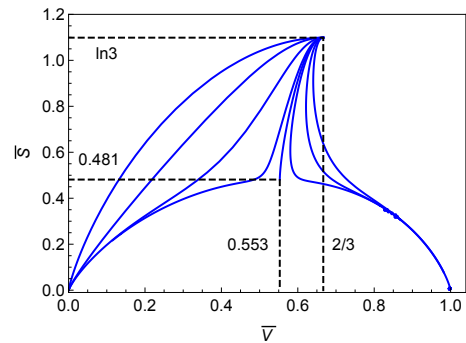


FIG. 15: Entropy \bar{S} versus excess volume \bar{V} for fixed values $\Gamma_S = 0, 1, 2, 2.8, 3, 3.2, 4, 5$ (from left to right).

effect that the excess volume initially increases from the value produced by the most disordered macrostate, but then turns around and increases. This effect is clearly observable in Fig. 15, which shows entropy versus excess volume. It is remarkably similar to Fig. 8 even though the large and small disks act quite differently.

IX. ALTERNATIVE PARTICLES

If gravity can be neglected, as is the case when the plane of the channel is oriented horizontally, the analysis requires no more than two species of particles, constructed from the tiles listed in Table I. The specifications of the two compacts are shown in Table V. These compacts are activated from the twofold degenerate pseudo-vacuum,

$$pv = \{vwvw \dots v, 4545 \dots 4\}. \quad (27)$$

Each compact particle has two distinct motifs. However, only one or the other motif will fit into a given slot. Each compact can be directly followed by a compact of the same species or the other species with exactly one motif fitting. All microstates that can be constructed under these rules have no more than three successive disks touching the same wall and then always with the small disk in the middle, which ensures mechanical stability.

TABLE V: Two species of compact quasi-particles. The motifs are for $\sigma_L = 2$, $\sigma_S = 1.4$, $H = 2.5$. The ID lists the overlapping tiles involved. The excess volume is ΔV_m and the activation energy ϵ_m .

motif	ID	m	category	ΔV_m	ϵ_m
	3v, w1	1	compact	V_t	pV_t
	25, 46	2	compact	V_t	pV_t

TABLE VI: Capacity constants A_m and statistical interaction coefficients $g_{mm'}$ for the particles from Table V.

m	A_m	$g_{mm'}$	1	2
1	$N-1$	1	1	0
2	$N-1$	2	1	1

Solving Eqs. (11) and (12) with β from (6) and substituting the results into (9) and (10) reproduces the population densities,

$$\bar{N}_1 = \bar{N}_2 = \frac{1}{2}\bar{V}, \quad (28)$$

for the two species of compacts and the identical relation (19b) between entropy and excess volume as previously obtained from four hosts and one tag.

X. CONCLUSION AND OUTLOOK

The work reported in this paper employs a methodology not commonly in use for jammed granular matter – a methodology shown here and earlier [70, 71] to deliver exact results for nontrivial scenarios. It promises to do the same for more complex scenarios. The focus here on disks of two sizes and weights has illuminated the workings of the exact analysis for specific situations.

The interplay between geometry, energetics, and combinatorics is encoded in a set of nonlinear equations for the jammed macrostates. Of the four types of relevant forces in the system under scrutiny here, the steric forces govern the mechanically stable configurations after jamming, whereas the pressure against mobile pistons, the gravitational force, and imposed random agitations govern the spatial configurations prior to jamming. The latter three are encoded in dimensionless parameters, by which all jammed macrostates are characterized.

The volume and entropy of macrostates, determined by their average particle content, become functions of the dimensionless parameters. The gradual variation of these parameters is akin to a quasistatic process described by variables analogous to thermodynamic functions. Some of these processes are found to encounter singularities reminiscent of phase transitions. A distinctive feature of jammed macrostates is that the same volume and entropy can be produced with very different contents of statistically interacting particles.

One extension of the work reported here which will cover much new ground permits random sequences of large and small disks of different weights. This scenario requires a different jamming protocol, where random agitations take place in a wider channel that allows disks to move past each other.

If we allow, in the jammed state, multiple small disks to be placed in sequence, the more stringent geometric

constraints,

$$\frac{1}{1 + \sqrt{3/4}} < \frac{\sigma_S}{\sigma_L} \leq 1, \quad (29a)$$

$$\frac{\sigma_L}{\sigma_S} < \frac{H}{\sigma_S} < 1 + \sqrt{3/4}, \quad (29b)$$

must be satisfied, replacing the condition (1). The number of distinct tiles that are realized is doubled from 8 in Table I to 16 in Table VII. The six distinct volumes of the 16 tiles are compiled in Table VIII

TABLE VII: Distinct tiles that constitute jammed microstates of arbitrary disk sequences subject to the constraints (2). Rule: v must be followed by w or 2 etc. Icons: $\sigma_L = 2$, $\sigma_S = 1.4$, $H = 2.5$. Rule amendments in square-brackets apply in the presence of centrifugal forces.

motif	ID	rule	vol.	motif	ID	rule	vol.
	1	2, 6, 10, 14	V_a		9	1, 5, [9]	V_d
	2	1, 5, 9, 13	V_a		10	2, 6, [10]	V_d
	3	4, 8, 12, 16	V_b		11	3, 7, 15, [11]	V_e
	4	3, 7, 11, 15	V_b		12	4, 8, 16, [12]	V_e
	5	4, 8, 12, 16	V_c		13	3, 7, 15, [11]	V_f
	6	3, 7, 11, 15	V_c		14	4, 8, 16, [12]	V_f
	7	2, 6, 10, 14	V_c		15	1, 5	V_f
	8	1, 5, 9, 13	V_c		16	2, 6	V_f

TABLE VIII: Volume of tiles assuming that the channel has unit cross sections. The numerical values pertain to the icons: $\sigma_L = 2$, $\sigma_S = 1.4$, $H = 2.5$.

	vol.	num.
V_a	$\sigma_L + \sqrt{H(2\sigma_L - H)}$	3.963
V_b	$\sigma_S + \sqrt{H(2\sigma_S - H)}$	2.266
V_c	$\frac{1}{2}(\sigma_L + \sigma_S) + \sqrt{H(\sigma_L + \sigma_S - H)}$	3.2
V_d	$2\sigma_L$	4.0
V_e	$2\sigma_S$	2.8
V_f	$\frac{1}{2}(\sigma_L + \sigma_S) + \sqrt{\sigma_L\sigma_S}$	3.373

Constructing a set of statistically interacting particles from this set of 16 tiles with the given successor rules that ensure mechanical stability under jamming is challenging task with no guarantee of success, in general.

However, in this instance we can take advantage of a mapping between this system of jammed disk and a spin- $\frac{3}{2}$ Ising chain, which was previously investigated by the same method [80] and shown to represent a system of statistically interacting particles from a set of 17 species.

The mapping is exact if we relax the successor rules in Table VII to include the entries in square brackets. This is justified if we consider channels that rotate about their axis and thus produce centrifugal forces on the disks [87]. The mapping also requires a switch from an open system

(grandcanonical ensemble) realized in the Ising context to a closed system (canonical ensemble) in the jammed-disk context, which requires the introduction of what in a thermodynamic system are chemical potentials. The ground is thus cleared for the exact analysis of a system of jammed granular matter with a random mix of grains of two different sizes. At the same time, a new path opens up for the study of particle segregation [88–90] with this methodology.

-
- [1] J. B. Knight, C. G. Fandrich, C. N. Lau, H. M. Jaeger, and S. R. Nagel, Density relaxation in a vibrated granular material, *Phys. Rev. E* **51**, 3957 (1995).
- [2] H. A. Makse, D. L. Johnson, and L. M. Schwartz, Packing of compressible granular materials, *Phys. Rev. Lett.* **84**, 4160 (2000).
- [3] V. Trappe, V. Prasad, L. Cipelletti, P. N. Segre, and D. A. Weitz, Jamming phase diagram for attractive particles, *Nature* **411**, 772 (2001).
- [4] F. Lechenault, F. da Cruz, O. Dauchot, and E. Bertin, Free volume distribution and compactivity measurement in a bidimensional granular packing, *J. Stat. Mech.* **P07009** (2006).
- [5] M. Schröter, S. Nägle, C. Radin, and H. L. Swinney, Phase transition in a static granular system, *Europhys. Lett.* **78**, 44004 (2007).
- [6] T. S. Majumdar, M. Sperl, S. Luding, and R. P. Behringer, Jamming transition in granular systems, *Phys. Rev. Lett.* **98**, 058001 (2007).
- [7] G.-J. Gao, J. Blawdziewicz, C. S. O’Hern, and M. Shattuck, Experimental demonstration of nonuniform frequency distributions of granular packings, *Phys. Rev. E* **80**, 061304 (2009).
- [8] Z. Zhang, N. Xu, D. T. N. Chen, P. Yunker, A. M. Alsayed, K. B. Aptowicz, P. Habdas, A. J. Liu, S. R. Nagel, and A. G. Yodh, Thermal vestige of the zero-temperature jamming transition, *Nature* **459**, 230 (2009).
- [9] J. Zhang, T. S. Majumdar, M. Sperl, and R. P. Behringer, Jamming for a 2D granular material, *Soft Matter* **6**, 2982 (2010).
- [10] K. A. Newhall, I. Jorjadze, E. Vandem-Eijnden, and J. Brujic, A statistical mechanics framework captures the packing of monodisperse particles, *Soft Matter* **7**, 11518 (2011).
- [11] K. V. Edmond, C. R. Nugent, and E. R. Weeks, Influence of confinement on dynamical heterogeneities in dense colloidal samples, *Phys. Rev. E* **85**, 041401 (2012).
- [12] J. G. Puckett and K. E. Daniels, Equilibrating temperaturelike variables in jammed granular subsystems, *Phys. Rev. Lett.* **110**, 058001 (2013).
- [13] E. S. Bililign, J. E. Kollmer, and K. E. Daniels, Protocol dependence and state variables in the force-moment ensemble, *Phys. Rev. Lett.* **122**, 038001 (2019).
- [14] C. S. O’Hern, S. A. Langer, A. J. Liu, and S. R. Nagel, Force distributions near jamming and glass transition, *Phys. Rev. Lett.* **86**, 111 (2001).
- [15] C. S. O’Hern, S. A. Langer, A. J. Liu, and S. R. Nagel, Random packings of frictionless particles, *Phys. Rev. Lett.* **88**, 075507 (2002).
- [16] N. Xu, J. Blawdziewicz, and C. S. O’Hern, Random close packing revisited: ways to pack frictionless disks, *Phys. Rev. E* **71**, 061306 (2005).
- [17] H. P. Zhang and H. A. Makse, Jamming transition in emulsions and granular materials, *Phys. Rev. E* **72**, 011301 (2005).
- [18] T. Unger, J. Kertesz, and D. E. Wolf, Force indeterminacy in the jammed state of hard disks, *Phys. Rev. Lett.* **94**, 178001 (2005).
- [19] M. Skoge, A. Donev, F. H. Stillinger, and S. Torquato, Packing hyperspheres in high-dimensional Euclidean spaces, *Phys. Rev. E* **74**, 041127 (2006).
- [20] A. Donev, F. H. Stillinger, and S. Torquato, Do binary hard disks exhibit an ideal transition? *Phys. Rev. Lett.* **96**, 225502 (2006).
- [21] G.-J. Gao, J. Blawdziewicz, and C. S. O’Hern, Frequency distribution of mechanically stable disk packings, *Phys. Rev. E* **74**, 061304 (2006).
- [22] S. Ostojic, E. Somfai, and B. Nienhuis, Scale invariance and universality of force networks in static granular matter, *Nature* **439**, 828 (2006).
- [23] E. Somfai, M. van Hecke, W. G. Ellenbroek, K. Shundyak, and W. van Saarloos, Critical and noncritical jamming of frictional grains, *Phys. Rev. E* **75**, 020301(R) (2007).
- [24] C. Song, P. Wang, and H. A. Makse, A phase diagram for jammed matter, *Nature* **453**, 629 (2008).
- [25] D. A. Head, Critical scaling and aging in cooling systems near the jamming transition, *Phys. Rev. Lett.* **102**, 138001 (2009).
- [26] K. W. Desmond and E. R. Weeks, Random close packing of disks and spheres in confined geometries, *Phys. Rev. E* **80**, 051305 (2009).
- [27] Y. Jin, P. Charbonneau, S. Meyer, C. Song, and F. Zamponi, Application of Edwards’ statistical mechanics to high-dimensional jammed sphere packings, *Phys. Rev. E* **82**, 051126 (2010).
- [28] M. Pica Ciamarra, a. Coniglio, and A. de Candia, Disordered jammed packings of frictionless spheres, *Soft Matter*, **6**, 2975 (2010).
- [29] Y. Jin and H. A. Makse, A first-order phase transition defines the random close packing of hard spheres, *Physica A* **389**, 5362 (1989).
- [30] C. F. Schreck, C. S. O’Hern, and L. E. Silbert, Tuning jammed frictionless disk packings from isostatic to hyperstatic, *Phys. Rev. E* **84**, 011305 (2011).
- [31] N. Xu, D. Frenkel, and A. J. Liu, Direct determination of the size of basins of attraction of jammed solids, *Phys. Rev. Lett.* **106**, 245502 (2011).

- [32] M. Otsuki and H. Hayakawa, Critical scaling near jamming transition for frictional granular particles, *Phys. Rev. E* **83**, 051301 (2011).
- [33] M. Pica Ciamarra, R. Pastore, M. Nicodemi, and A. Coniglio, Jamming phase diagram for frictional particles, *Phys. Rev. E* **84**, 041308 (2011).
- [34] R. Pastore, M. Pica Ciamarra, and A. Coniglio, Absence of fragility and mechanical response of jammed granular matter, *Granular Matter* **14**, 253 (2012).
- [35] P. Charbonneau, E. I. Corwin, G. Parisi, and F. Zamponi, Universal microstructure and mechanical stability of jammed packings, *Phys. Rev. Lett.* **109**, 205501 (2012).
- [36] R. Hihinashvili and R. Blumenfeld, Statistical-mechanical characteristics of dense granular matter, *Granular Matter* **14**, 277 (2012).
- [37] S. Lévy, D. Fischer, R. Stannarius, B. Szabó, T. Börzsönyi, and J. Török, Frustrated packing in a granular system under geometrical confinement. *Soft Matter* **14**, 396 (2018).
- [38] H. M. Jaeger and S. R. Nagel, Granular solids, liquids, and gases, *Rev. Mod. Phys.* **68**, 129 (1996).
- [39] P. G. de Gennes, Granular matter: a tentative view, *Rev. Mod. Phys.* **71**, S374 (1999).
- [40] H. A. Makse, J. Brujic, and S. F. Edwards, Statistical mechanics of jammed matter, in *The physics of granular matter*, H. Hinrichsen and D. E. Wolf (Eds.), Wiley-VCH (2005).
- [41] Anita Mehta, Spatia, dynamical and spatiotemporal heterogeneities in granular media, *Soft Matter* **6**, 2875 (2010).
- [42] S. Torquato and F. H. Stillinger, Jammed hard-particle packings: from Kepler to Bernal and beyond, *Rev. Mod. Phys.* **82**, 2633 (2010).
- [43] N. Xu, Mechanical, vibrational, and dynamical properties of amorphous systems near jamming, *Front. Phys.* **6**, 109 (2011).
- [44] A. Baule, F. Morone, H. J. Herrmann, and H. A. Makse, Edwards statistical mechanics for jammed granular matter, *Rev. Mod. Phys.* **90**, 015006 (2018).
- [45] R. P. Behringer and B. Chakraborty, The physics of jamming for granular materials: a review, *Rep. Prog. Phys.* **82**, 012601 (2019).
- [46] S. F. Edwards and R. B. S. Oakeshott, Theory of powders, *Physica A* **157**, 1080 (1989).
- [47] A. Mehta and S. F. Edwards, Statistical mechanics of powder mixtures, *Physica A* **157**, 1091 (1989).
- [48] C. C. Mounfield and S. F. Edwards, The statistical mechanics of granular systems composed of elongated grains, *Physica A* **210**, 279 (1989).
- [49] S. F. Edwards and C. C. Mounfield, The statistical mechanics of granular systems composed of spheres and elongated grains, *Physica A* **210**, 290 (1989).
- [50] S. F. Edwards and D. V. Grinev, Compactivity and transmission of stress in granular materials, *Chaos* **9**, 551 (1999).
- [51] S. F. Edwards, The distribution of forces in a granular system under external stress is a spinglass problem, *J. Phys. A: Math. Theor.* **41**, 324019 (2008).
- [52] R. Blumenfeld and S. F. Edwards, On granular stress statistics: compactivity angoricity, and some open issues, *J. Phys. Chem. B* **113**, 3981 (2009).
- [53] K. Wang, C. Song, P. Wang, and H. A. Makse, Edwards thermodynamics of the jamming transition for frictionless packings: ergodicity test and role of angoricity and compactivity, *Phys. Rev. E* **86**, 011305 (2012).
- [54] R. C. Ball and R. Blumenfeld, Stress field in granular systems: loop forces and potential formulation, *Phys. Rev. Lett.* **88**, 115505 (2002).
- [55] F. H. Stillinger, H. Sakai, and S. Torquato, Lattice-based random jammed configurations for hard particles, *Phys. Rev. E* **67**, 031107 (2003).
- [56] R. Blumenfeld and S. F. Edwards, Granula entropy: explicit calculations for planar assemblies, *Phys. Rev. Lett.* **90**, 114303 (2003).
- [57] C. Briscoe, C. Song, P. Wang, H. A. Makse, Entropy of jammed matter, *Phys. Rev. Lett.* **101**, 188001 (2008).
- [58] C. Briscoe, C. Song, P. Wang, H. A. Makse, Jamming III: characterizing randomness via the entropy of jammed matter, *Physica A* **389**, 3978 (2010).
- [59] M. Danisch, Y. Jin, and H. A. Makse, Model of random packings of different size balls, *Phys. Rev. E* **81**, 051303 (2010).
- [60] C. Song, P. Wang, Y. Jin, and H. A. Makse, Jamming I: a volume function for jammed matter, *Physica A* **389**, 4497 (2010).
- [61] S. Meyer, C. Song, Y. Jin, K. Wang, and H. A. Makse, Jamming in two-dimensional packings, *Physica A* **389**, 5137 (2010).
- [62] E. DeGiuli and J. McElwaine, Laws of granular solids: geometry and topology, *Phys. Rev. E* **84**, 041310 (2011).
- [63] J. M. Luck and A. Mehta, Dynamical diversity and metastability in a hindered granular column near jamming, *Eur. Phys. J. B* **57**, 429 (2007).
- [64] J. M. Luck and A. Mehta, The effects of grain shape and frustration in a granular column near jamming, *Eur. Phys. J. B* **77**, 505 (2010).
- [65] R. K. Bowles and I. Saika-Voivod, Landscapes, dynamic heterogeneity, and kinetic facilitation in a simple off-lattice model, *Phys. Rev. E* **73**, 011503 (2006).
- [66] S. S. Ashwin and R. K. Bowles, Complete jamming landscapes of confined hard discs, *Phys. Rev. Lett.* **102**, 235701 (2009).
- [67] R. K. Bowles and S. S. Ashwin, Edwards entropy and compactivity in a model of granular matter, *Phys. Rev. E* **83**, 031302 (2011).
- [68] M. Z. Yamchi, S. S. Ashwin, and R. K. Bowles, Fragile-strong fluid crossover and universal relaxation times in a confined hard-disk fluid, *Phys. Rev. Lett.* **109**, 225701 (2012).
- [69] S. S. Ashwin, M. Z. Yamchi, and R. K. Bowles, Inherent structure landscape connection between liquids, granular materials, and the jamming phase diagram, *Phys. Rev. Lett.* **110**, 145701 (2013).
- [70] N. Gundlach, M. Karbach, D. Liu, and G. Müller, Jammed disks in a narrow channel: criticality and ordering tendencies, *J. Stat. Mech.* P04018 (2013).
- [71] C. Moore, D. Liu, B. Ballnus, M. Karbach, G. Müller, Disks in a narrow channel jammed by gravity and centrifuge: profiles of pressure, mass density and entropy density, *J. Stat. Mech.* P04008 (2014).
- [72] F. D. M. Haldane, *Fractional statistics in arbitrary dimensions: a generalization of the Pauli principle*, *Phys. Rev. Lett.* **67**, 937 (1991).
- [73] Y.-S. Wu, *Statistical distribution for generalized ideal gas of fractional-statistics particles*, *Phys. Rev. Lett.* **73**, 922 (1994).
- [74] S. B. Isakov, *Statistical mechanics for a class of quantum*

- statistics, Phys. Rev. Lett. **73**, 2150 (1994); *Generalization of statistics for several species of identical particles*, Mod. Phys. Lett. B **8**, 319 (1994).
- [75] D.-V. Anghel, *The thermodynamic limit for fractional exclusion statistics*, J. Phys. A **40**, F1013 (2007); *The fractional exclusion statistics amended*, Europhys. Lett. **87**, 60009 (2009).
- [76] G. A. Nemnes and D.-V. Anghel, *Fractional exclusion statistics in non-homogeneous interacting particle systems*, Roman. Rep. Phys. **66**, 336 (2014).
- [77] P. Lu, J. Vanasse, C. Piecuch, M. Karbach, and G. Müller, *Statistically interacting quasiparticles in Ising chains*, J. Phys. A **41**, 265003 (2008).
- [78] D. Liu, P. Lu, G. Müller, and M. Karbach, *Taxonomy of particles in Ising spin chains*, Phys. Rev. E **84**, 021136 (2011).
- [79] P. Lu, D. Liu, G. Müller, and M. Karbach, *Interlinking motifs and entropy landscapes of statistically interacting particles*, Condens. Matter Phys. **15**, 13001 (2012) [arXiv:1108.2990].
- [80] D. Liu, J. Vanasse, G. Müller, and M. Karbach, *Generalized Pauli principle for particles with distinguishable traits*, Phys. Rev. E **85**, 011144 (2012).
- [81] G. G. Potter, G. Müller, and M. Karbach, *Thermodynamics of ideal quantum gas with fractional statistics in D dimensions*, Phys. Rev. E **75**, 061120 (2007); *Thermodynamics of statistically interacting quantum gas in D dimensions*, **76**, 061112 (2007).
- [82] P. Lu, G. Müller, and M. Karbach, *Quasiparticles in the XXZ model*, Condensed Matter Physics, **12**, 381 (2009) [arXiv:0909:2728].
- [83] G. P. Sharma, Y. K. Reshetnyak, O. A. Andreev, M. Karbach, and G. Müller, *Coil-helix transition of polypeptide at water-lipid interface*, J. Stat. Mech. **P01034** (2015).
- [84] A. C. Meyer, Y. Öez, N. Gundlach, M. Karbach, P. Lu, and G. Müller, *Molecular chains under tension: thermal and mechanical activation of statistically interacting extension and contraction particles*, Phys. Rev. E **101**, 022504 (2020).
- [85] D. Liu and G. Müller, *Jammed disks of two sizes in a narrow channel*, In: I. Zuriguel, A. Garcimartin, and R. Cruz (Eds.) *Traffic and Granular Flow 2019*, Springer Proceedings in Physics, **252**, 389 (2019).
- [86] The zero gravity limit can be implemented by tilting the plane of the channel from vertical toward horizontal.
- [87] The relaxed successor rules in Table VII can be eliminated in two ways: (i) by freezing out specific particle species (lifting their activation energies to infinity), (ii) by converting tag particles into cap particles [80].
- [88] C. M. Dury, and G. H. Ristow, *Radial segregation in a two-dimensional rotating drum*, J. Phys I France **7**, 737 (1997).
- [89] G. C. M. A. Ehrhardt, A. Stephenson, and P. M. Reis, *Segregation mechanism in a numerical model of a binary granular mixture*, Phys. Rev. E **71**, 041301 (2005).
- [90] J. M. N. T. Gray, *Particle segregation in dense granular flow*, Ann. Rev. Fluid Mech. **50**, 407 (2018).